Journal of Power Sources 195 (2010) 7349–7358

Contents lists available at ScienceDirect

Journal of Power Sources

journal homepage: www.elsevier.com/locate/jpowsour

Passive cathodic water/air management device for micro-direct methanol fuel cells

Hsien-Chih Peng[a], Po-Hon Chen[a], Hung-Wen Chen[a], Ching-Chang Chieng[a], Tsung-Kuang Yeh[a,c], Chin Pan[a], Fan-Gang Tseng[a,b,*]

[a] Department of Engineering and System Science, National Tsing Hua University, Taiwan, ROC
[b] Division of Mechanics, Research Center for Applied Sciences, Academia Sinica, Taiwan, ROC
[c] Nuclear Science and Technology Development Center, National Tsing Hua University, 101, Sec. 2, Kuang Fu Rd., Hsinchu 300, Taiwan, ROC

ARTICLE INFO

Article history:
Received 10 April 2010
Accepted 4 May 2010
Available online 12 May 2010

Keywords:
Fuel cells
Cathode water removal
Water/air management
V-groove micro-channel
Corner flow

ABSTRACT

A high efficient passive water/air management device (WAMD) is proposed and successfully demonstrated in this paper. The apparatus consists of cornered micro-channels and air-breathing windows with hydrophobicity arrangement to regulate liquids and gases to flow on their predetermined pathways. A high performance water/air separation with water removal rate of about 5.1 $\mu l\,s^{-1}\,cm^{-2}$ is demonstrated. The performance of the proposed WAMD is sufficient to manage a cathode-generated water flux of 0.26 $\mu l\,s^{-1}\,cm^{-2}$ in the micro-direct methanol fuel cells (μDMFCs) which are operated at 100 mW cm^{-2} or 400 mA cm^{-2}. Furthermore, the condensed vapors can also be collected and recirculated with the existing micro-channels which act as a passive water recycling system for μDMFCs. The durability testing shows that the fuel cells equipped with WAMD exhibit improved stability and higher current density.

1. Introduction

Portable electronic and electromechanical devices have become increasingly popular in recent years. A portable, charge-free, and compact power supply system that can promptly provide electrical energy is therefore highly demanded. Micro-direct methanol fuel cells (μDMFCs) with high theoretical energy density hold great promise to provide the ultimate solution.

The chemical energy within the methanol can be converted into electrical energy directly. The electrochemical reactions can be described as follows:

$$CH_3OH + H_2O \rightarrow 6e^- + 6H^+ + CO_2\uparrow \quad \text{(anodic side)}$$

$$1.5O_2 + 6e^- + 6H^+ \rightarrow 3H_2O \quad \text{(cathodic side)}$$

$$CH_3OH + 1.5O_2 \rightarrow 2H_2O + CO_2 \quad \text{(overall reaction)}$$

According to the above reactions, CO_2 bubbles and water are generated at the anode and cathode, respectively. At high power output condition, the cathode product (H_2O) will be generated in liquid form that quickly accumulates and clogs up the reaction area, resulting in the blockage of oxygen pathways, and simultaneously retards the cathode reduction process. Moreover, H_2O can be easily transported from the anode by protons through the membrane [1]. It is essential for a quick removal of the water droplets to maintain a high cell performance. Therefore, the water removal rate should outperform the water flooding rate at cathode during the operation of DMFCs. In fact, water can be removed by either air flow [2–4] or electro-osmosis pumping [5]. However, these active water removal methods are not favorable for μDMFC systems, since it consumes electric power and increases the system size. Therefore, it is highly desirable to develop a passive water management device for μDMFCs.

Recently, many researchers have employed various methods to remove micro-water droplets by wettability gradients based on micro-structures and chemical gradients for fuel cells passively. For example, a micro-hole array structure with alternative hydrophilic and hydrophobic surfaces was proposed [6]. The cathode-generated water can be driven passively into the hydrophilic area, thus the hydrophobic area can provide a diffusion path for oxygen. Water droplets from condensed vapor and CO_2 bubbles can also be manipulated and separated on anode surface with a wettability gradient of a μDMFC [7]. In addition, the combined hydrophilic micro-channels and hydrophobic nano-porous membrane facilitates the fuel circulation at anode with CO_2 bubbles acting as the driving force. This configuration can effectively reduce the size of gas separating and pumping system [8–10]. The

* Corresponding author at: Engineering and System Science Department, National Tsing Hua University, 101, Sec. 2, Kuang-fu Rd., Hsinchu 30013, Taiwan, R.O.C. Tel.: +886 3 5715131x34270; fax: +886 3 5733054.
E-mail address: fangang@ess.nthu.edu.tw (F.-G. Tseng).

0378-7753/$ – see front matter © 2010 Elsevier B.V. All rights reserved.
doi:10.1016/j.jpowsour.2010.05.007

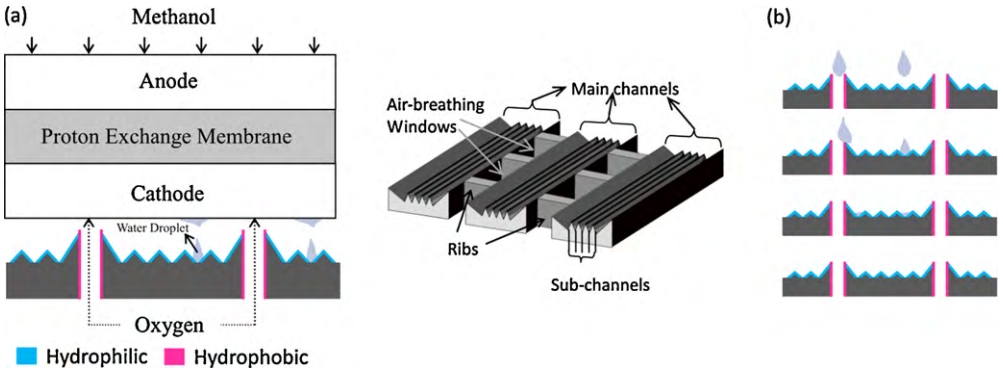

Fig. 1. (a) The schematic diagram of a water/air management device (WAMD) for micro-direct methanol fuel cells. (b) The moving sequence of droplets on WAMD.

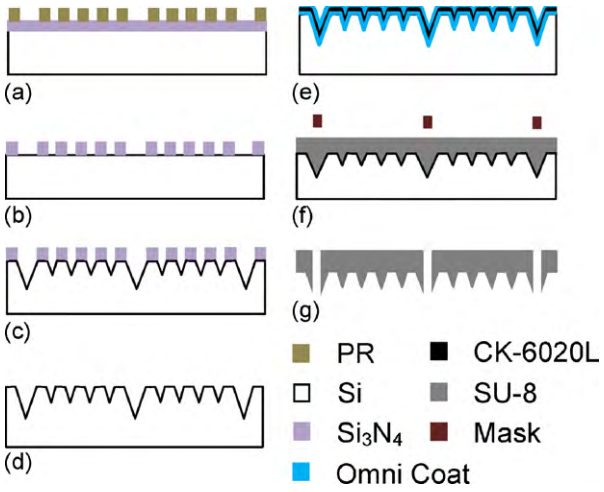

Fig. 2. Fabrication process flow of the WAMD. (a) Si_3N_4 pattern definition, (b) Si_3N_4 etched by RIE, (c) Si etched by KOH, (d) Si_3N_4 removed by RIE, (e) adhesion/release layer (OmniCoat) and the anti-reflection resist (CK-6020L) coatings, (f) SU8 spin-coating and UV exposure, and (g) releasing.

cathode-generated water can also be passively removed from the reaction area by applying tapered channels with surface wettability gradient on the channel wall at the cathode [11]. The aforementioned methods have demonstrated impressive capability on water removal. However, their performance has not yet been compared to the practical requirement in water management at cathode of a μDMFC. In this study, we propose the use of an array of corner-type micro-channels incorporated with partial hydrophobic treatment on the rib structures as an alternative way for rapid water removal at the cathode of a μDMFC while maintaining a high ratio of gas pathway for rapid air convection.

2. Design and fabrication

2.1. Design concept

The water volume flux Q in the cathode of a μDMFC can be expressed as follows:

$$Q = \frac{\gamma m}{\rho} \quad (1)$$

where γ is the water (H_2O) molecules generation rate per second, m and ρ are the molecular weight and the density of H_2O, respectively. According to the electrochemical reaction at cathode, the ratio of electrons to H_2O molecules is 2 to 1. At a current output of 100 mA, the electron generation rate is $6.25 \times 10^{17}\ s^{-1}$. Therefore, γ at 100 mA will be 3.125×10^{17} molecules s^{-1}, while ρ and m are $1\ g\ ml^{-1}$ and $2.99 \times 10^{-23}\ g\ molecule^{-1}$, respectively. Based on the above parameters, Q can be estimated as $9.34 \times 10^{-6}\ ml\ s^{-1}$.

Previous study has found that almost $3H_2O$ molecules could be dragged across the membrane from anode to cathode as a result of electro-osmosis effect [1]. For this reason, there is an additional volume flux of H_2O at cathode. Under the 100 mA condition, the additional amount of H_2O due to electro-osmotic will be 6-fold the H_2O generated from the cathodic reaction. Therefore, the real water volume flux Q_{real} will be $(1+6) \times 9.34 \times 10^{-6}\ ml\ s^{-1} = 0.0654\ \mu l\ s^{-1}$.

Recently, Lu and Wang [12] and Wong et al. [13] presented high performance μDMFCs with a peak power density of 100 mW and a related current density of 400 mA cm^{-2}. As a result, the water generation rate under this condition will be $0.26\ \mu l\ s^{-1}\ cm^{-2}$, which is 4-fold the Q_{real}. Therefore, the design of the water/air management device (WAMD) will aim to accommodate at least one order of magnitude higher than the reported Q for a μDMFC that operates under 100 mW.

In the current design of the WAMD, the major driving force is originated from the capillary effect in v-groove channels [14]. Considering the contact angle θ between the fluid and side wall, and the half angle α of the v-groove corner, droplets can be

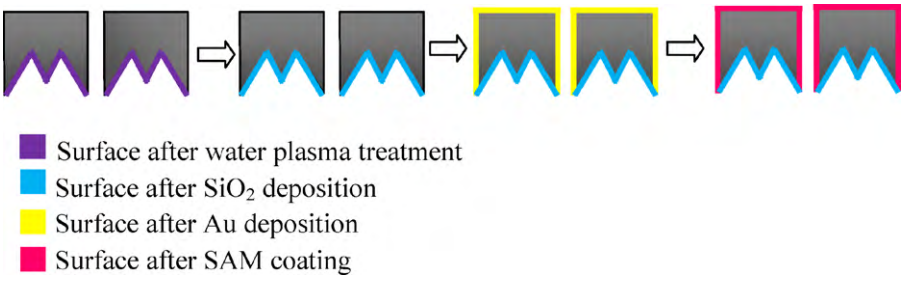

Fig. 3. Wettability modification processes for WAMD.

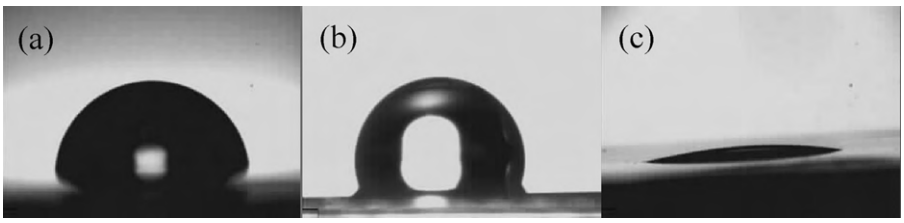

Fig. 4. Contact angles of different surface wettability on (a) SU8, 84°, (b) SU8 with SAM coating, 105° and (c) SU8 with 1500 Å SiO_2 coating, 13°.

spontanously sucked into the corner of the channel as soon as it touches the channel wall if the v-groove angle (2α) satisfies the Concus–Finn condition, $\theta < (\pi/2) - \alpha$. In order to accommodate this concept for rapid water removal with air pathway as large as possible, the WAMD is designed and equipped on the cathode as schematically shown in Fig. 1(a). Main channels, ribs, and air-breathing windows are regularly networked in the structure for water removal, structural support, and air (or oxygen) passage of the cathode, respectively. The surfaces of the channels and the air-breathing windows are treated to become hydrophilic and hydrophobic, respectively. The sub-channels of the WAMD that are faced to the cathode surface with a gap of about 100 μm. As the cathode-generated droplets come in contact with the device, the droplets can be passively driven to the hydrophilic areas, dragged toward the corners of the sub-channels, and finally transported to the borders of the device for storage or recycling, as shown in Fig. 1(b). The windows/channels ratio of 40% is designed such that 8.16×10^{-5} mol cm^{-2} s^{-1} of oxygen can reach the electrode by convection and diffusion under a 400 mA cm^{-2} output current condition, and the cross-sectional area of the v-groove channel regions in 1 cm^2 of WAMD is 9.375×10^{-4} cm^2 cm^{-2}. As a result, a water flow rate of 0.27 cm s^{-1} is required to effectively remove the water from cathode that generates water at a rate of 0.26 μl s^{-1} cm^{-2} as previously estimated to prevent flooding. This flow rate can be easily achieved by setting $\alpha = 70°$ and $\theta < 15°$ at the same time.

2.2. Device fabrication

The detailed process flow of the WAMD is illustrated in Fig. 2. A Si(1 0 0) wafer was first cleaned by RCA process before the deposition of 500 Å silicon nitride (Si_3N_4) by a low pressure chemical vapor deposition (LPCVD) system as shown in Fig. 2(a). Afterward, v-shape grooves were fabricated by KOH etching after patterning of Si_3N_4 by reactive ion etching (RIE) [14] (Fig. 2(b) and (c)), and the structured Si mold was obtained right after the residues of Si_3N_4 were thoroughly removed (Fig. 2(d)). A negative photoresist (SU-8 2035) was employed as the casting material. In order to facilitate the release process and to prevent the reflection effect during UV exposure processes, XP OmniCoat adhesion/release layer (MicroChem Corp., USA), anti-reflection resist (CK-6020L; Fuji Film Olin Inc., Japan) and XP OmniCoat adhesion/release layer were coated onto the Si mold sequentially (Fig. 2(e)). The structures, channels (for water delivery), and windows (for air-breathing) were defined accordingly after UV exposure and subsequent curing and releasing processes (Fig. 2(f) and (g)). To prevent the interference between water and air, the surfaces of the channels and the windows were modified to exhibit hydrophilic and hydrophobic properties, respectively.

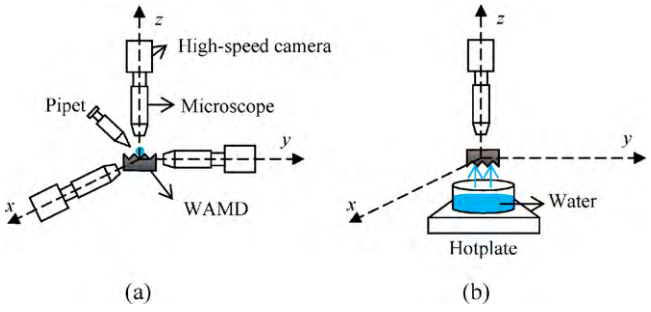

Fig. 6. Experimental setups for (a) droplet test and (b) vapor test. In droplet test, pipette dispensing was employed to mimic water generation from cathode and the droplet behaviors in WAMD was recorded from 3 different directions (X, Y, and Z). In vapor test, water evaporation method was used to mimic the vapor generated in cathode and the condensed vapor behaviors was recorded from the backside of the WAMD.

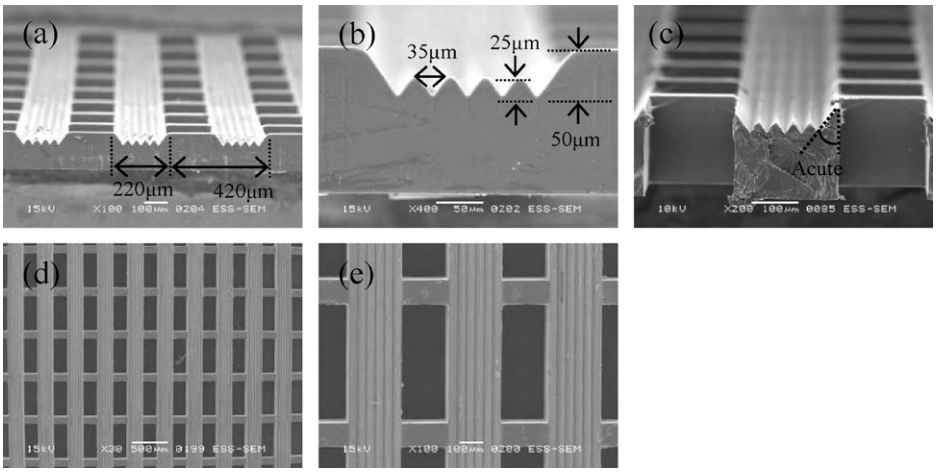

Fig. 5. SEM images of the water/air management device (WAMD). (a) Side view of main channel; (b and c) enlarged side views of the main channel on the rib and window sections, respectively; (d) top view of the device; (e) enlarged top view area. The windows/channels ratio is about 40%.

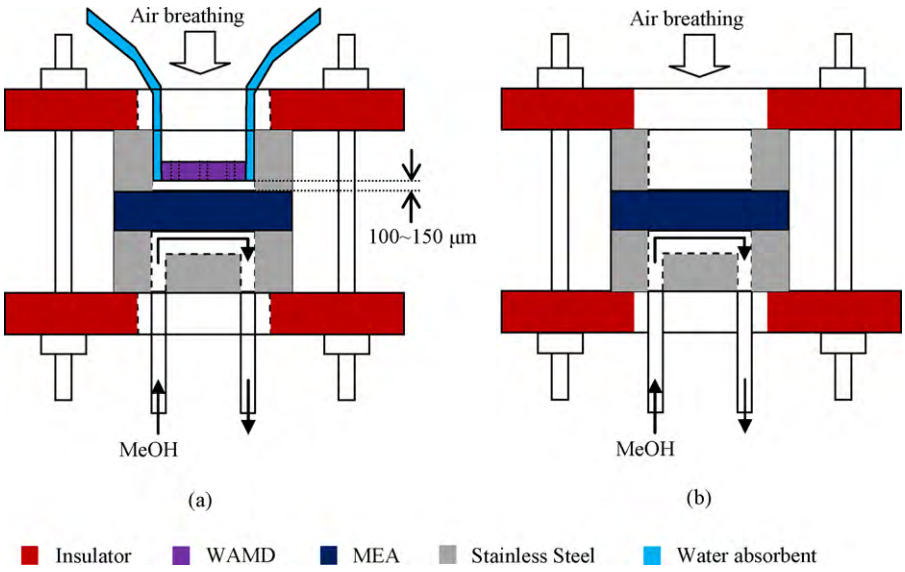

Fig. 7. The two tested fuel cell systems. (a) WAMD-equipped system; (b) reference system without WAMD.

Fig. 3 shows the detailed surface treatment procedures. The channels were first treated with water plasma to activate the surface. Then, 1500 Å SiO_2 was deposited on the surface by electron-beam evaporation system to achieve hydrophilicity. Afterward, 200 Å Ti and 300 Å Au were deposited sequentially on the remaining sides of the structure, including the surface of the windows by electron-beam evaporation system. Eventually, designated hydrophobic surfaces can be achieved after immersing the structure into a thiol-based self-assembled monolayer (SAM) ($C_{18}H_{38}S$, 1-octadecanethiol 98%, Aldrich Inc., USA) [15] for 24 h. Fig. 4 shows the respective contact angles of the surfaces of as-fabricated SU-8 (Fig. 4(a)), SAM coated SU-8 (Fig. 4(b)) and SiO_2 coated SU-8 (Fig. 4(c)) at 84°, 105° and 13°. Fig. 5 shows the SEM images of the as-fabricated WAMD. Main channels are connected by the ribs with a pitch of 420 μm, and the windows/channels ratio is about 40%. There are almost 24 main channels within 1 cm in length (24 main channels cm^{-1}), and each main channel is composed of 5 sub-channels (v-groove channels). Fig. 5(a) and (b) show the cross-sectional images cutting through the rib while Fig. 5(c) shows the cross-sectional image cutting through window. Note that an acute profile at the interface between the channel and window can be clearly seen in Fig. 5(c), which is important for the droplet removal and will be discussed in detail in the next section.

2.3. Experimental

Since most of the electrodes in DMFCs are made of carbon clothes, water droplets can easily adhere on the fibers within the clothes as a result of surface tension force [16]. The experimental setup to study the droplet emerging process on carbon clothes

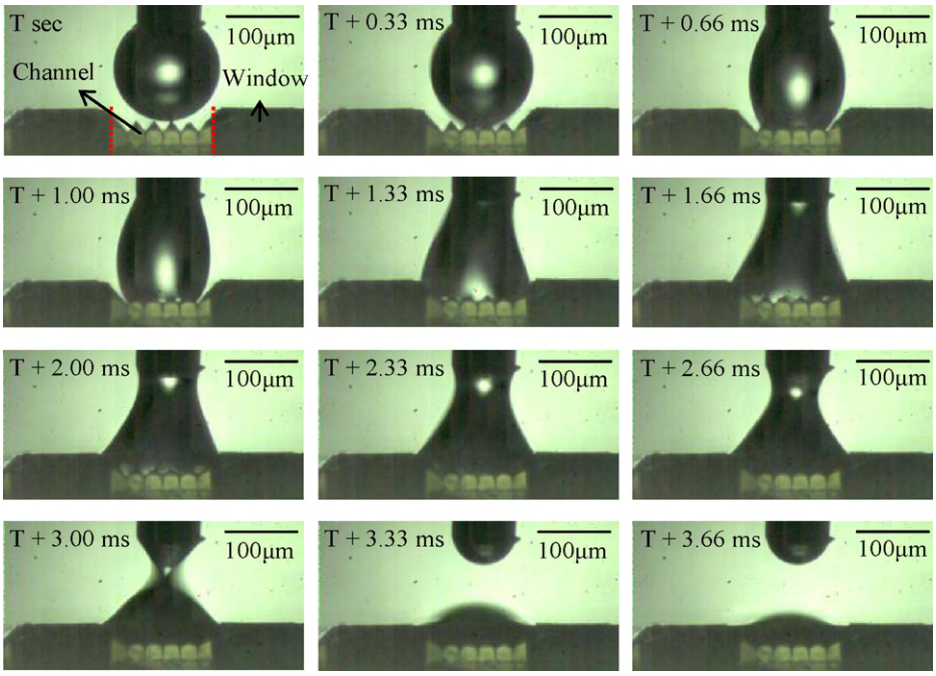

Fig. 8. The side view (X-direction) of the droplet which is touching the top of the channel (see online resource 1).

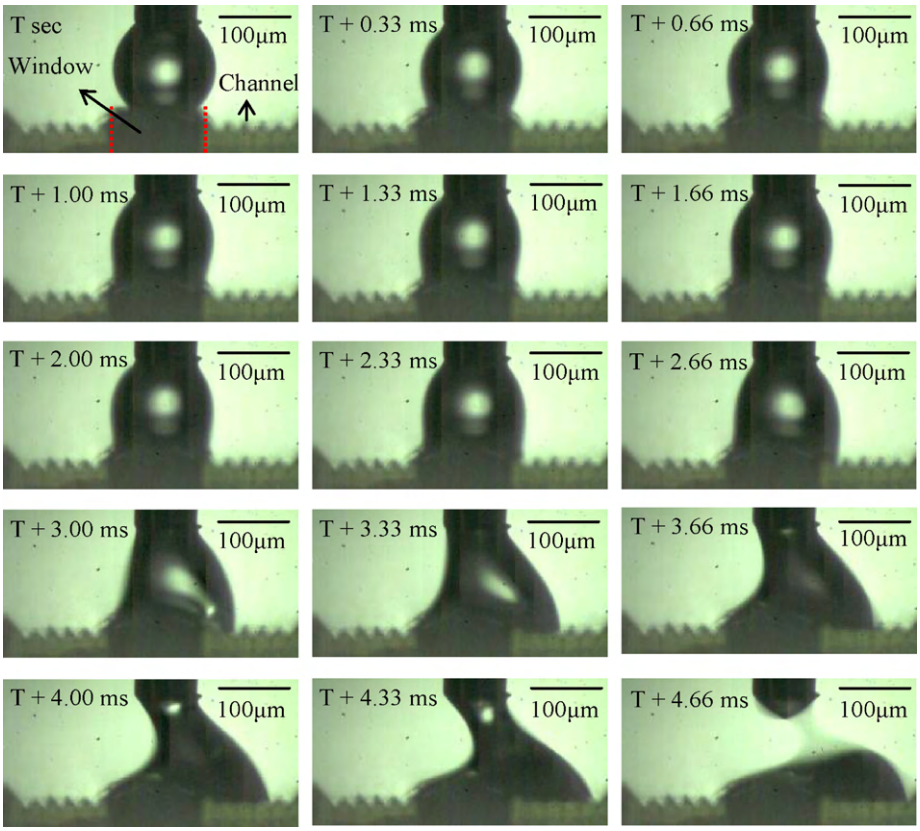

Fig. 9. Side view (X-direction) of the droplet which is touching the top of the window (see online resource 2).

in DMFCs is schematically shown in Fig. 6. The time evolutions of the droplets being dispensed in the channels were recorded by a high-speed camera (FASTCAM APX, Photron, USA) from three different views. The main channels of the WAMD were aligned along the X-axis while the v-groove tips of the sub-channels were directed towards the Z-axis as shown in Fig. 6. Fixed-volume of water droplets was dispensed from a pipette tip to the channel surface of the WAMD. The time evolutions of droplet-channel inter-

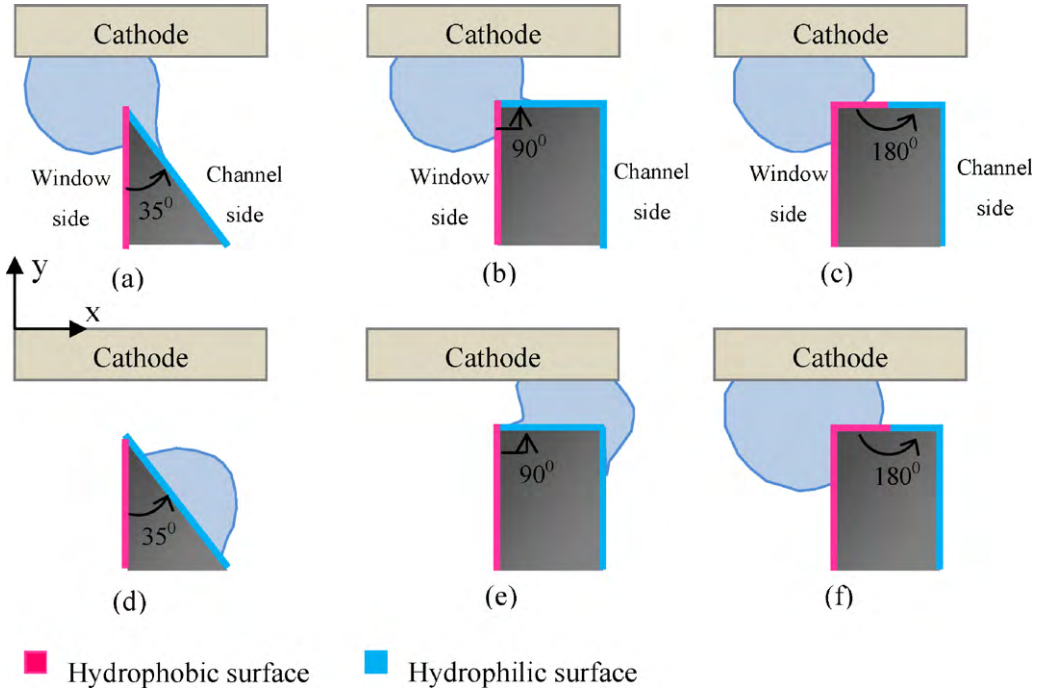

Fig. 10. The schematic diagram of droplet removal processes on different structural configurations with predetermined wetting properties. (a) Acute shape, 30°; (b) right-angle shape, 90°; (c) planar shape, 180°. The droplet behaviors on different shapes are compared in (d)–(f), and it can be concluded that the acute structure provides the best performance in term of droplet removability.

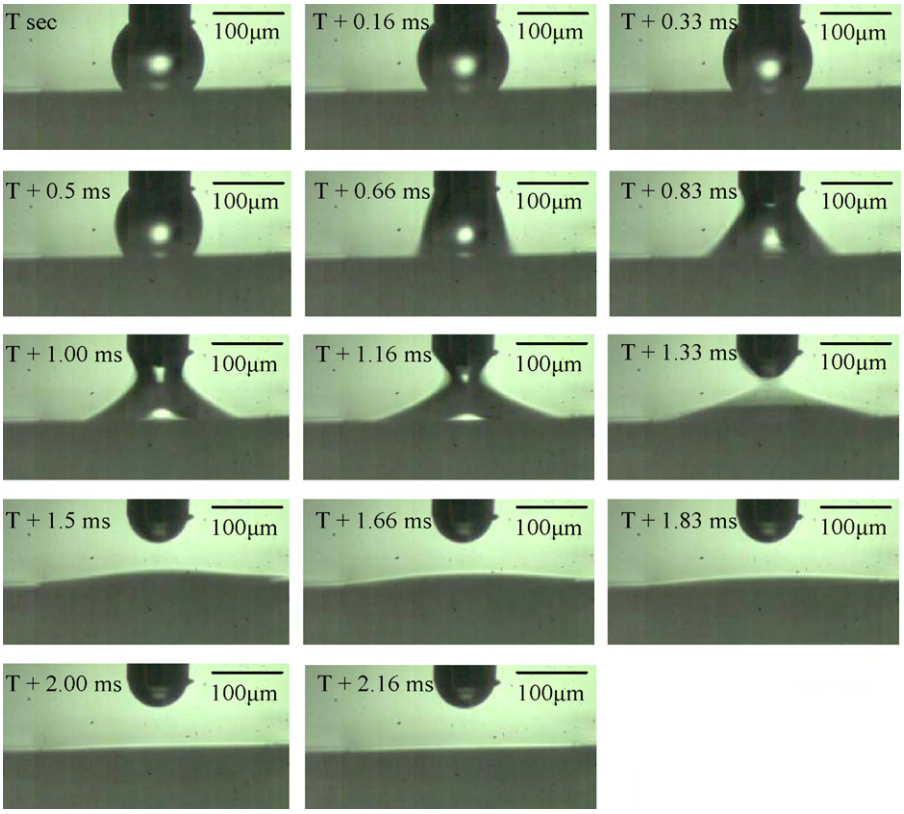

Fig. 11. Side view (Y-direction) of the droplet which is touching the top of the WAMD (see online resource 3).

action were recorded from X-, Y-, and Z-axes, respectively. On the other hand, in order to understand the global effect when multiple droplets appeared on the WAMD surface simultaneously and continuously, a water vapor generation system was employed to mimic the condition. The nucleation, growth, coalescence, and the flow of water droplets were all recorded by high-speed camera for detailed analysis. The fuel cell durability tests were also carried out in this study. The carbon clothes were used at the anode (EC-CC1-060) and cathode (EC-CC12-060T) to support catalysts. Two different mixtures of 29 wt% Pt–15.25 wt% Ru on Vulcan XC-72 carbon black (Johnson Matthey Fuel Cells Co. Ltd.) and 20 wt% Pt on Vulcan XC-72 carbon black (BASF Fuel Cell Inc.) were used as the catalysts for the cathode and anode, respectively. These catalysts were then mixed with a 5 wt% liquid Nafion each time they were deposited on the carbon clothes by spray method. The catalyst loading was 1 mg cm^{-2} Pt and 0.5 mg cm^{-2} Ru for the anode and 1 mg cm^{-2} Pt for the cathode. A membrane electrode assembly (MEA) was formed by sandwiching a Nafion membrane (Nafion-117, DuPont) between the anode and cathode and hot pressing them at 120 °C and 150 kgf cm^{-2} for 10 min. In order to assemble a complete fuel cell system, the MEA was sandwiched by two stainless steel plates for electron conducting and fuel transporting. A 1 M methanol (MeOH) solution was then fed to the anode with a flow rate of 2 ml min^{-1} and the cathode was exposed to the ambient condition with the cell operated at room temperature. The effective reaction area was 0.44 cm^2. Fig. 7(a) shows a WAMD-equipped fuel cell system. The WAMD was fixed on a stainless steel plate with a distance about 100–150 μm from the cathodic electrode and a water-absorbent cotton strip was located at the end of the channels of the WAMD to absorb water which was transported from the channels. Fig. 7(b) is a reference system which was equipped without a WAMD nor water absorbents for comparison. The performance of both fuel cell systems is then discussed in the next section.

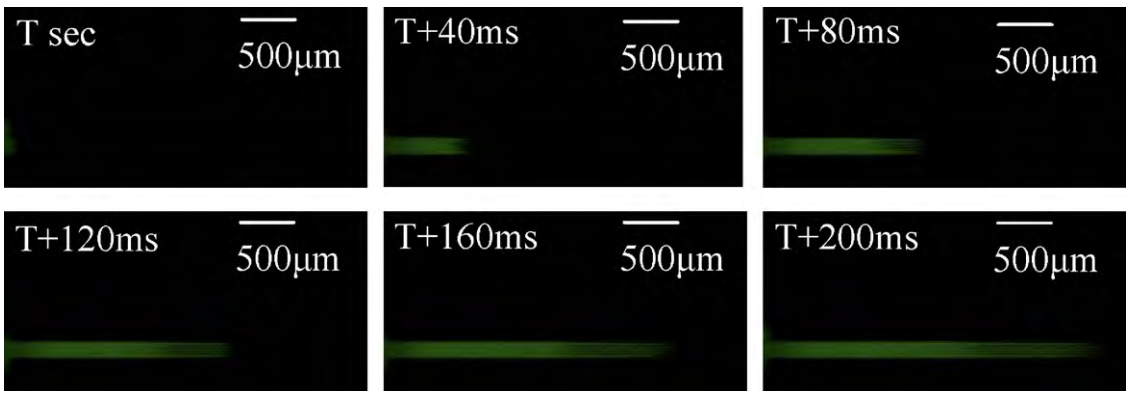

Fig. 12. Top view (Z-direction) of the fluorescent molecule liquid droplet moving in one main channel of WAMD (see online resource 4).

3. Results and discussion

3.1. Droplet moving test

3.1.1. Side view (X-, Y-direction)

Fig. 8 shows the evolution process of a 0.1 μl droplet dispensed into one of the WAMD main channels. Images were captured from X-direction. The droplet departed from the tip within 3 ms and spread into the channel immediately. It shows that the surface tension force during the droplet contacts with the channel is large enough to separate the droplet from the pipette. This complete process was documented with a video (300-fold slower than the original) (see online resource 1). In addition, a droplet was dispensed to the top of the window intentionally to confirm that a water clog-free window exists during the operating process. The images in Fig. 9 were captured from X-direction when the droplet touched the window. This complete process was also documented with a video (300-fold slower than the original) (see online resource 2). Clearly, the droplet can spontaneously move to the channel owing to the large difference surface condition between the sidewall of the window and the channel. This result assures that droplets can always be swept away wherever droplets emerge. Moreover, it should be noted that the acute profile at the hydrophilic/hydrophobic boundary yields better droplet removal capability.

Consider the different configurations of hydrophilic/hydrophobic interfaces, e.g. acute apex, right-angle corner, and planar shape, as shown in Fig. 10(a)–(c), different droplet removal abilities can be carried out. The liquid that appears at the hydrophobic area will not be removed away until it reaches the hydrophobic/hydrophilic interface. Assume a fixed volume of droplets approaches the hydrophobic areas for each structure type, droplets will soon touch the hydrophobic/hydrophilic interface and move toward the hydrophilic area in both the apex and right-angle structures, as shown in Fig. 10(d) and (e). However, the droplet in Fig. 10(f) will not be removed until the droplet is large enough to touch the hydrophobic/hydrophilic wetting boundary

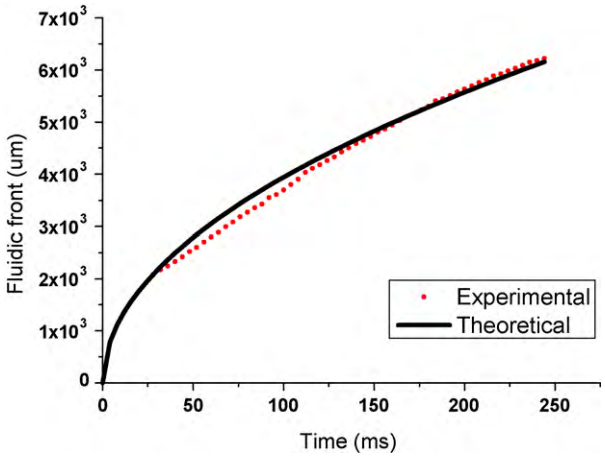

Fig. 13. The relationship between fluidic front and time traveled. Red dots represent the experimental data and the black line represents the theoretical data. (For interpretation of the references to color in this figure legend, the reader is referred to the web version of the article.)

and therefore it will impede the cathodic reaction in practical use. Though the droplets in the apex and right-angle structures can be quickly driven towards the hydrophilic area, their behaviors are different. In Fig. 10(d), the droplet will quickly leave the electrode as soon as it touches the apex, since the electrode surface will help the crossover of the droplet into the hydrophilic region. However, the droplet that appears at the right-angle structure will be confined in the gap between the structure and electrode, as shown in Fig. 10(e). Thus, the reaction area of cathode will be occupied during the droplet transport. Hence, it is concluded that the acute profile design at the hydrophilic/hydrophobic boundary in this research is more efficient for droplet removal.

The behavior of 0.1 μl droplet observed from the Y-direction is shown in Fig. 11. The water flowed towards both ends of the channel and spread symmetrically within 2.16 ms. This complete

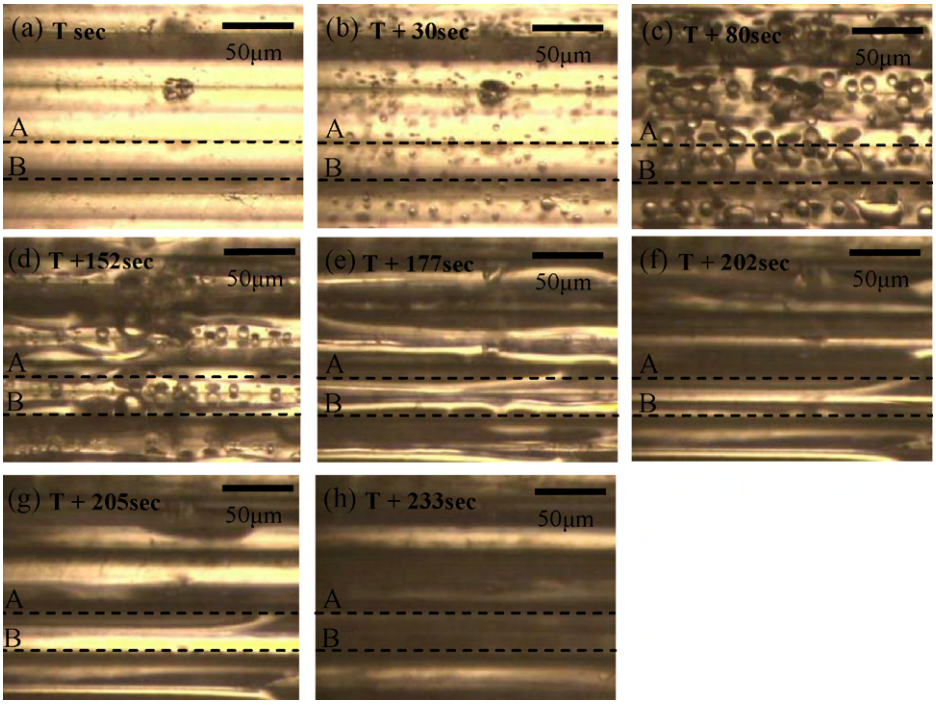

Fig. 14. Top view (Z-direction) of the condensed vapor evolution in WAMD. Dashed lines A and B indicate the peak and valley in the channel, respectively (see online resource 6).

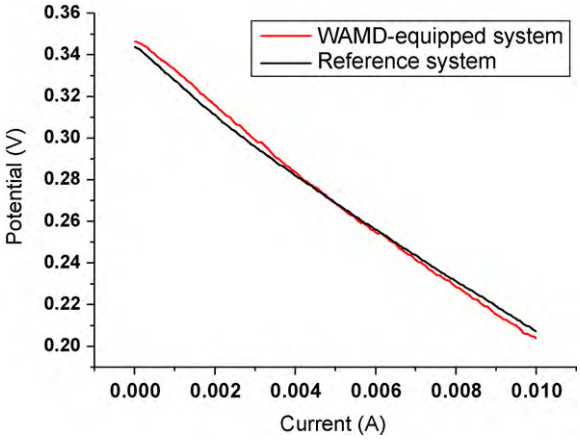

Fig. 15. The polarization characteristics of both fuel cell testing systems. Red and black solid lines represent the WAMD-equipped and reference systems, respectively. (For interpretation of the references to color in this figure legend, the reader is referred to the web version of the article.)

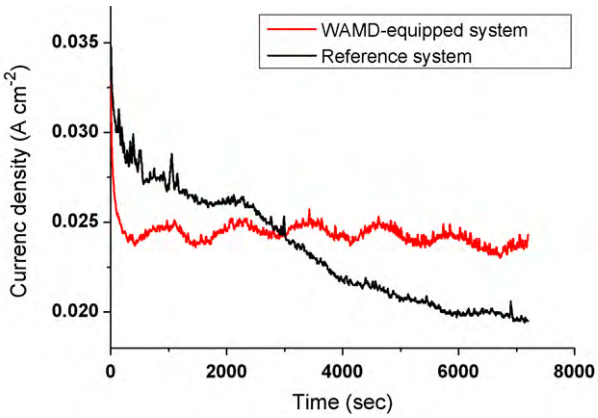

Fig. 16. The durability testing results of both fuel cell systems. Red and black solid lines represent the WAMD-equipped and reference systems, respectively. (For interpretation of the references to color in this figure legend, the reader is referred to the web version of the article.)

process was documented with a video (300-fold slower than the original) (see online resource 3). It shows that the hydrophilic surface treatment based on the deposition of SiO_2 by electron-beam evaporation is uniform and reliable inside the v-groove channels.

3.1.2. Top view (Z-direction)

The top view images of droplet evolutions inside WAMD were recorded to determine *Q*. Since the backside of the channel was covered by opaque Au thin film, the fluidic behaviors can only be observed by fluorescent microscopy from the top view.

Fig. 12 shows the progression of a 0.2 μl fluorescent (fluorescein sodium salt, SIGMA Inc., USA) droplet inside a main channel. This complete process was again documented with a video (10-fold slower than the original) (see online resource 4). The water front traveled 4.3 mm in 200 ms and the average velocity was about 21.5 mm s^{-1}. Mathematical models have been developed by Weislogel and Lichter [17] to describe corner flows that are confined by different boundary conditions. In this paper, the channel boundary condition of a constant height was adopted. The relationship between fluidic moving distance and time can be represented by the following equation [17]:

$$L = 1.702\, G^{1/2} H^{1/2} t^{1/2} \quad (2)$$

where *L* is the forefront of the flow, the constant value of 1.702 is derived by employing the constant height condition to the invariant similarity equation, *G* is the related fluidic coefficient that equals to 2.144 (see supplementary information), *H* and *t* are the height of the channel and the time required to travel at a certain distance, respectively. In this case, $H = 25\ \mu m$. The experimental data was compared with the theoretical results in Fig. 13 and good agreement between the experimental and theoretical results has been

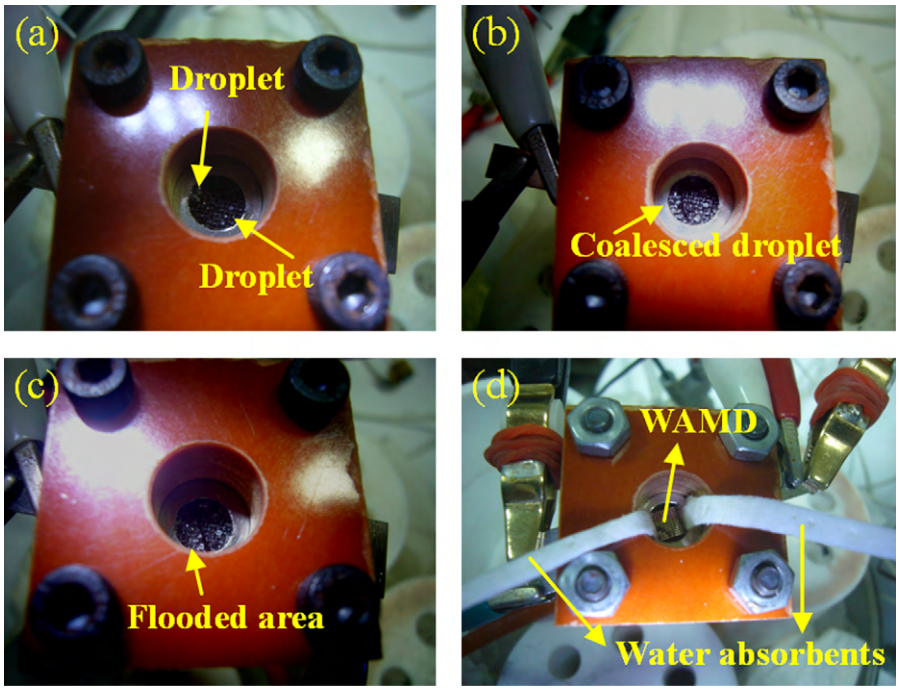

Fig. 17. The images of the cathode of the reference system operated at (a) 1800 s, (b) 3600 s, and (c) 7200 s. (d) The image of the cathode of the WAMD-equipped system during operation.

achieved. The formula was originally verified in mm scale, and here, the results showed that the theory was also valid in μm regime.

Furthermore, the Q in the main channel can be estimated through multiplying the main channel cross-sectional area (7.062×10^{-3} mm^2) by the flow velocity (21.5 mm s^{-1}), and it equals to 0.151 μl s^{-1}. Since there are 24 channels cm^{-1} of WAMD, the passively removed water flux can also be estimated as 5.1 μl s^{-1} cm^{-2}. The estimated flow rate is 20 times higher than 0.26 μl s^{-1} cm^{-2} of the DMFC water generation flux that is operated at 400 mA cm^{-2}. The complete fluid flow process was documented with a video (10-fold slower than the original) (see online resource 5). It demonstrates that the windows are always clog-free wherever the droplets are dispensed at.

3.2. Condensed vapor test

Since the anode fuel is usually a dilute methanol; therefore, cathode-generated water can be recycled as the solvent for methanol. Yao et al. [18] proposed a method that the cathode-generated water can be pumped back to the anode to dilute methanol. The water captured by WAMD of this research can also be collected and pumped back to anode for recycling purpose. The behaviors of the vapor condensation in the channel of WAMD were observed from the backside of the WAMD. Therefore, the deposition of Au and subsequent SAM coating was omitted in the current test on WAMD structure to provide a clear optical pathway for observation. Fig. 14 shows the vapor behaviors in the channel of WAMD. Dashed lines A and B indicate the peak and valley of the channel, respectively. The vapor condensation rate was estimated as 2.33×10^{-9} μl s^{-1}. Initially, random droplet nucleation and coalescence on the channel surface were observed (Fig. 14(a) and (b)). Some droplets started to merge to a larger one as soon as they came in contact with each other (Fig. 14(c)). The coalesced droplets continued to grow up and then fill into the v-groove channels. This process forced the droplets to elongate and turn into a stream in the channel (Fig. 14(d)–(h)). Eventually, all condensed vapor could be collected or recycled as the solvent of anode fuel. The process went in cycles with further vapor feeding. It took 233 s to remove the first condensed droplets and then only 15 s to remove the follow-up condensing droplets. The complete process was documented with a video (10-fold faster than the original) (see online resource 6).

3.3. Fuel cell operating tests

The polarization characteristics of both the WAMD-equipped and reference fuel cell systems are shown in Fig. 15. The red and black solid lines in Fig. 15 represent the WAMD-equipped and reference systems, respectively. It was found that there was no obvious difference between the two systems. Since the current was scanned from the open circuit voltage (0.34 V) to 0.2 V and the scan rate was 0.01 mA s^{-1}, the water flooding issue could not be seen under this testing condition. Therefore, a durability test was carried out to verify the efficiency of the WAMDs. Continuous data of the output current was recorded while a 0.2 V constant voltage was extracted from the fuel cell system. The current–time plot was shown in Fig. 16 with the red and black solid lines represent the WAMD-equipped and the reference systems, respectively. The results show that almost 43% current reduction was found in the reference system but only a 26% current reduction was found in the WAMD-equipped system instead. The 43% current reduction of the reference system was attributed to the problem of water flooding, as shown in Fig. 17. Fig. 17(a)–(c) shows the images of the cathode of the reference system when the system continuously operated at 1800 s, 3600 s and 7200 s, respectively. Random water droplet formation was found at 1800 s as shown in Fig. 17(a), and then the droplets grew, coalesced and submerged parts of the cathodic reaction area at 3600 s as shown in Fig. 17(b). At 7200 s, almost half the cathodic reaction area was flooded, comparable to the percentage of the current reduction observed. In the testing of the WAMD-equipped system, initially the current declined during the first 300 s, but after the decline, it remained stable showing a continuous slight periodic oscillation until the end of the test. Fig. 17(d) shows the image of a WAMD-equipped fuel cell system during operation. A WAMD was located in the middle of the cathodic reaction area while water-absorbent cotton strips were connected to both ends of the channels of the WAMD. The WAMD and water-absorbent cotton strips covered parts of the reaction area. Therefore, the steep current reduction of the WAMD-equipped system could be attributed to the two reasons mentioned above. However, a stable current signal of the WAMD-equipped system was observed during the durability test. The standard deviation of the current density was only 0.46 mA cm^{-2} from 300 s to 7200 s. Moreover, a periodic current cycle with duration of 1200 s was also noticed in the WAMD-equipped system. Based on the results, since the droplets were continuously generated at the cathode, according to the droplet moving test, it was believed that the droplets can be effectively removed by the WAMD when they reached a critical size.

4. Conclusion

An effective water/air management device (WAMD) for μDMFCs was designed and fabricated successfully by SU-8 molding and selective surface modification processes. The system yielded a water removal rate of 5.1 μl s^{-1} cm^{-2}, which is about 20 times much faster than the water generation rate of a μDMFC operated at 400 mA cm^{-2}. Droplets were quickly removed wherever the droplets emerged due to the strong wettability gradient at the hydrophobic/hydrophilic interface exactly located at an acute junction. For water recycling, not only water but also vapor generated droplets were collected in the current WAMD design. When the vapor was consecutively fed onto WAMD, the condensed vapor droplets coalesced with each other and flowed toward the ends of the channel in cycles. Each periodic cycle took about 15 s after the process reached a steady state. The fuel cell system exhibited improved durability and more stable current output when the system was equipped with a WAMD.

Acknowledgements

The authors would like to thank National Science Council of Taiwan for the financial support (NSC 98-3114-E-007-009, NSC 97-2623-7-007-012-ET, NSC 96-2218-E-007-008). The authors also acknowledge helpful discussion with Dr. Hwa Seng Khoo.

Appendix A. Supplementary data

Supplementary data associated with this article can be found, in the online version, at doi:10.1016/j.jpowsour.2010.05.007.

References

[1] X. Ren, S. Gottesfeld, J. Electrochem. Soc. 148 (2001) A87–A93.
[2] B. Bae, B.K. Kho, T.-H. Lim, I.-H. Oh, S.-A. Hong, H.Y. Ha, J. Power Sources 158 (2006) 1256–1261.
[3] N. Nakagawa, Y. Xiu, J. Power Sources 118 (2003) 248–255.
[4] C.Y. Chen, P. Yang, J. Power Sources 123 (2003) 37–42.
[5] C.R. Buie, J.D. Posner, T. Fabian, C.A. Suk-Won, D. Kim, F.B. Prinz, J.K. Eaton, J.G. Santiago, J. Power Sources 161 (2006) 191–202.
[6] Y. Alyousef, S.C. Yao, Microfluid Nanofluidics 2 (2006) 337–344.
[7] Y.J. Chuang, C.C. Chieng, C. Pan, S.J. Luo, F.G. Tseng, J. Micromech. Microeng. 17 (2007) 915–922.

[8] D.D. Meng, C.J. Kim, J. Power Sources 194 (2009) 445–450.
[9] D.D. Meng, T. Cubaud, C.-M. Ho, C.-J. Kim, J. Microelectromech. Syst. 16 (2007) 1403–1410.
[10] D.D. Meng, J. Kim, C.-J. Kim, J. Micromech. Microeng. 16 (2006) 419–424.
[11] T. Metz, N. Paust, C. Müller, R. Zengerle, P. Koltay, Sens. Actuators A: Phys. 143 (2008) 49–57.
[12] G.Q. Lu, C.Y. Wang, J. Fuel Cell Sci. Technol. 3 (2006) 131–136.
[13] C.W. Wong, T.S. Zhao, Q. Ye, J.G. Liu, J. Power Sources 155 (2006) 291–296.
[14] G.P. Peterson, A.B. Duncan, M.H. Weichold, J. Heat Transfer 115 (1993) 751–756.
[15] Y. Li, K.-S. Moon, C.P. Wong, J. Electron. Mater. 34 (2005) 266–271.
[16] G.Q. Lu, C.Y. Wang, J. Power Sources 134 (2004) 33–40.
[17] M.M. Weislogel, S. Lichter, J. Fluid Mech. 373 (1998) 349–378.
[18] S.-C. Yao, X. Tang, C.-C. Hsieh, Y. Alyousef, M. Vladimer, G.K. Fedder, C.H. Amon, Energy 31 (2006) 636–649.